J|A|C|S
ARTICLES

$[Mn^{III}_4Ln^{III}_4]$ Calix[4]arene Clusters as Enhanced Magnetic Coolers and Molecular Magnets

Georgios Karotsis,[†] Stuart Kennedy,[‡] Simon J. Teat,[§] Christine M. Beavers,[§] Drew A. Fowler,[||] Juan J. Morales,[⊥] Marco Evangelisti,*[,#] Scott J. Dalgarno,*[,‡] and Euan K. Brechin*[,†]

School of Chemistry, The University of Edinburgh, West Mains Road, Edinburgh EH9 3JJ, Scotland, U.K., School of Engineering and Physical Sciences—Chemistry, Heriot-Watt University, Riccarton, Edinburgh EH14 4AS, Scotland, U.K., Advanced Light Source, Lawrence Berkeley National Laboratory, 1 Cyclotron Road, MS 6R2100, Berkeley, California 94720, Department of Chemistry, University of Missouri, 601 South College Avenue, Columbia, Missouri 65211, and Departamento de Física de la Materia Condensada and Instituto de Ciencia de Materiales de Aragón, CSIC-Universidad de Zaragoza, 50009 Zaragoza, Spain

Received June 15, 2010; E-mail: evange@unizar.es; s.j.dalgarno@hw.ac.uk; ebrechin@staffmail.ed.ac.uk

Abstract: The use of methylene-bridged calix[4]arenes in 3d/4f chemistry produces a family of clusters of general formula $[Mn^{III}_4Ln^{III}_4(OH)_4(C4)_4(NO_3)_2(DMF)_6(H_2O)_6](OH)_2$ (where C4 = calix[4]arene; Ln = Gd (**1**), Tb (**2**), Dy (**3**)). The molecular structure describes a square of Ln^{III} ions housed within a square of Mn^{III} ions. Magnetic studies reveal that **1** has a large number of molecular spin states that are populated even at the lowest investigated temperatures, while the ferromagnetic limit $S = 22$ is being approached only at the highest applied fields. This, combined with the high magnetic isotropy, makes the complex an excellent magnetic refrigerant for low-temperature applications. Replacement of the isotropic Gd^{III} ions with the anisotropic Tb^{III} and Dy^{III} ions "switches" the magnetic properties of the cluster so that **2** and **3** behave as low-temperature molecular magnets, displaying slow relaxation of the magnetization.

Introduction

Magnetic refrigeration constitutes one of the potential applications envisioned for polymetallic molecules.[1] The magnetocaloric effect (MCE) is based on the change of magnetic entropy upon application of a magnetic field and is of great technological importance since it can be used for cooling applications according to a process known as adiabatic demagnetization.[2,3] This energy-efficient and environmentally friendly technique is particularly promising for refrigeration in the ultra-low-temperature region, providing, for example, a valid alternative to the use of ^{3}He, which is becoming rare and expensive.[4] Recent studies have demonstrated that the MCE of selected molecular cluster compounds can be much larger than that found in the best, and conventionally studied, intermetallic and lanthanide alloys and magnetic nanoparticles. The recipe[5] required for making such molecules requires them to have a negligible anisotropy, which therefore permits easy polarization of the net molecular spin, leading to a large magnetic entropy change and the presence of degenerate or low-lying excited spin states, since the so-added degrees of freedom result in extra magnetic entropy. In short, we must target high-spin (ferromagnetic) isotropic clusters displaying weak intramolecular magnetic exchange. The $[Mn_{12}]$ and $[Fe_8]$ molecular magnets were the first to be investigated for magnetic refrigeration because of their well-defined $S = 10$ ground states, and although they displayed relatively large $-\Delta S_m$ values, the large anisotropy present in both systems freezes the orientation of the molecular spins once the temperature is lowered below ~4 K, limiting their applicability.[1,6,7] The first isotropic molecular cluster studied was the heterometallic $[Cr_7Cd]$ wheel,[8] but the problem in this case was the low value of the spin, $S = 3/2$. A huge step

[†] The University of Edinburgh.
[‡] Heriot-Watt University.
[§] Lawrence Berkeley National Laboratory.
[||] University of Missouri.
[⊥] Departamento de Física de la Materia Condensada, Universidad de Zaragoza.
[#] Instituto de Ciencia de Materiales de Aragón, CSIC-Universidad de Zaragoza.

(1) (a) Spichkin, Yu. I.; Zvezdin, A. K.; Gubin, S. P.; Mischenko, A. S.; Tishin, A. M. *J. Phys. D: Appl. Phys.* **2001**, *34*, 1162. (b) Evangelisti, M.; Luis, F.; de Jongh, L. J.; Affronte, M. *J. Mater. Chem.* **2006**, *16*, 2534.
(2) See, for example: (a) Zimm, C.; Jastrab, A.; Sternberg, A.; Pecharsky, V. K.; Gschneidner, K. A., Jr.; Osborne, M.; Anderson, I. *Adv. Cryogen. Eng.* **1998**, *43*, 1759. (b) Pecharsky, V. K.; Gschneidner, K. A., Jr. *J. Magn. Magn. Mater.* **1999**, *200*, 44. (c) Gschneidner, K. A., Jr.; Pecharsky, A. O.; Pecharsky, V. K. In *Cryocoolers II*; Ross, R. S., Jr., Ed.; Kluwer Academic/Plenum Press: New York, 2001; p 433.
(3) (a) Debye, P. *Ann. Phys.* **1926**, *81*, 1154. (b) Giauque, W. F. *J. Am. Chem. Soc.* **1927**, *49*, 1864.
(4) Feder, T. *Phys. Today* **2009**, *62*, 21.
(5) Evangelisti, M.; Brechin, E, K. *Dalton Trans.* **2010**, *39*, 4672, and references therein.
(6) (a) Torres, F.; Hernández, J. M.; Bohigas, X.; Tejada, J. *Appl. Phys. Lett.* **2000**, *77*, 3248. (b) Torres, F.; Bohigas, X.; Hernández, J. M.; Tejada, J. *J. Phys.: Condens. Matter* **2003**, *15*, L119.
(7) Zhang, X. X.; Wei, H. L.; Zhang, Z. Q.; Zhang, L. *Phys. Rev. Lett.* **2001**, *87*, 157203.
(8) Affronte, M.; Ghirri, A.; Carretta, S.; Amoretti, G.; Piligkos, S.; Timco, G. A.; Winpenny, R.E. P. *Appl. Phys. Lett.* **2004**, *84*, 3468.

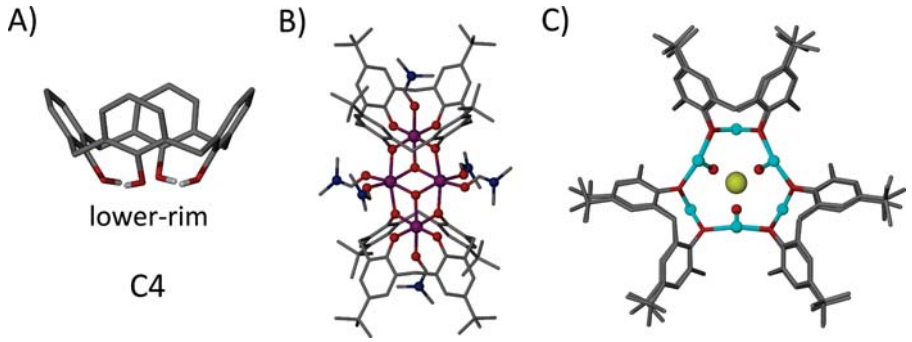

Figure 1. (A) Calix[4]arene, C4. (B) The $[Mn^{III}_2Mn^{II}_2]$ single-molecule magnet formed with TBC4.[20a] (C) View down the center of a tricapped trigonal prismatic enneanuclear Cu^{II} cluster formed with TBC4 that binds two chloride anions (one above and below the cluster core).[20b] Figures are not to scale. Hydrogen atoms are omitted for clarity (except for the lower-rim hydroxyl groups in panel A). Ligated solvent molecules and solvent of cocrystallization are omitted for clarity in panel C. Color code: Mn, purple; O, red; N, dark blue; C, gray; Cu, light blue; Cl, yellow.

forward in the search for truly applicable molecular candidates was accomplished via the synthesis and study of highly symmetric molecules with large values of the spin ground state. The first was $[Fe_{14}]$ with an $S = 25$ ground state,[9] the second a ferromagnetic $[Mn_{10}]$ supertetrahedron with $S = 22$, displaying practically zero anisotropy,[10] and the third a $[Mn_{14}]$ disk[11] displaying a truly enormous enhancement of the MCE with values of $-\Delta S_m$ as large as 25 J Kg^{-1} K^{-1} for liquid-helium temperatures and $\Delta B = 7$ T—almost a factor of 2 larger than that of $[DyCo_2]$ nanoparticles.[12] One of our long-standing synthetic strategies for making high-spin molecular clusters is the use of polyalkoxide ligands such as the tripodal 1,1,1-tris(hydroxymethyl)ethane, 1,1,1-tris(hydroxymethyl)propane, and pentaerythritol.[13] The disposition of the three alkoxide arms of the trianions of $RC(CH_2OH)_3$ pro-ligands directs the formation of triangular $[M_3]$ units where each arm of the ligand bridges one edge of the triangle. These triangular building blocks then self-assemble to form elaborate architectures (M_9 partial icosahedra,[14] M_{10} supertetrahdra,[10] Mn_{32} truncated cubes,[15] etc.) whose topologies are dependent on reaction conditions and/or the presence of other bridging and/or terminal coligands such as carboxylates, β-diketonates, etc.[13] A natural extension of this strategy is the use of tetrapodal alkoxides such as calix[4]arenes. Calix[4]arenes are cyclic molecules that have been used extensively in the formation of supramolecular structures and in various fields of coordination chemistry.[16] Calix[4]arene (C4, Figure 1A) is a cyclic polyphenol that is synthetically accessible on a large scale via the parent *p*-^{t}Bu derivative (TBC4),[17] and this molecule is the typical starting point for synthetic alteration to the general molecular framework.[18] In a bowl conformation, the calix[4]arene polyphenolic pocket at the lower rim is an attractive feature for metal complexation.[19] We[20] and others[21] have been using methylene-bridged calix[4]arenes for the construction of polynuclear metal clusters possessing interesting magnetic properties. Thia- and sulfonyl-bridged calix[4]arenes have also been used in this regard, but these molecules form distinctly different cluster motifs due to the bridging atoms taking part in the coordination chemistry of the resulting complexes.[22] With methylene-bridged TBC4, we have recently synthesized and characterized $[Mn^{III}_2Mn^{II}_2]$ single-molecule

(9) (a) Evangelisti, M.; Candini, A.; Ghirri, A.; Affronte, M.; Brechin, E. K.; McInnes, E. J. L. *Appl. Phys. Lett.* **2005**, *87*, 072504. (b) Low, D. M.; Jones, L. F.; Bell, A.; Brechin, E. K.; Mallah, T.; Rivière, E.; Teat, S. J.; McInnes, E. J. L. *Angew. Chem., Int. Ed.* **2003**, *42*, 3781. (c) Shaw, R.; Laye, R. H.; Jones, L. F.; Low, D. M.; Talbot-Eeckelaers, C.; Wei, Q.; Milios, C. J.; Teat, S. J.; Helliwell, M.; Raftery, J.; Evangelisti, M.; Affronte, M.; Collison, D.; Brechin, E. K.; McInnes, E. J. L. *Inorg. Chem.* **2007**, *46*, 4968.
(10) Manoli, M.; Johnstone, R. D. L.; Parsons, S.; Murrie, M.; Affronte, M.; Evangelisti, M.; Brechin, E. K. *Angew. Chem., Int. Ed.* **2007**, *46*, 4456.
(11) Manoli, M.; Collins, A.; Parsons, S.; Candini, A.; Evangelisti, M.; Brechin, E. K. *J. Am. Chem. Soc.* **2008**, *130*, 11129.
(12) Ma, S.; Cui, W. B.; Li, D.; Sun, N. K.; Geng, D. Y.; Jiang, X.; Zhang, Z. D. *Appl. Phys. Lett.* **2008**, *92*, 173113.
(13) Brechin, E. K. *Chem. Commun.* **2005**, 5141.
(14) (a) Brechin, E. K.; Soler, M.; Davidson, J.; Hendrickson, D. N.; Parsons, S.; Christou, G. *Chem. Commun.* **2002**, 2252. (b) Piligkos, S.; Rajaraman, G.; Soler, M.; Kirchner, N.; van Slageren, J.; Bircher, R.; Parsons, S.; Güdel, H.-U.; Kortus, J.; Wernsdorfer, W.; Christou, G.; Brechin, E. K. *J. Am. Chem. Soc.* **2005**, *127*, 5572.
(15) (a) Scott, R. T. W.; Parsons, S.; Murugesu, M.; Wernsdorfer, W.; Christou, G.; Brechin, E. K. *Angew. Chem., Int. Ed.* **2005**, *44*, 6540. (b) Evangelisti, M.; Candini, A.; Affronte, M.; Pasca, E.; de Jongh, L. J.; Scott, R. T. W.; Brechin, E. K. *Phys. Rev. B* **2009**, *79*, 104414.
(16) For example, see: (a) MacGillivray, L. R.; Atwood, J. L. *Nature* **1997**, *389*, 469. (b) Orr, G. W.; Barbour, L. J.; Atwood, J. L. *Science* **1999**, *285*, 1049. (c) Gerkensmeier, T.; Iwanek, W.; Agena, C.; Froehlich, R.; Kotila, S.; Nather, C.; Mattay, J. *Eur. J. Org. Chem.* **1999**, 2257. (d) Atwood, J. L.; Barbour, L. J.; Dalgarno, S. J.; Hardie, M. J.; Raston, C. L.; Webb, H. R. *J. Am. Chem. Soc.* **2004**, *126*, 13170. (e) Dalgarno, S. J.; Tucker, S. A.; Bassil, D. B.; Atwood, J. L. *Science* **2005**, *309*, 2037. (f) Ugono, O.; Holman, K. T. *Chem. Commun.* **2006**, 2144. (g) Barrett, E. S.; Dale, T. J.; Rebek, J., Jr. *J. Am. Chem. Soc.* **2007**, *129*, 3818.
(17) Gutsche, C. D. *Acc. Chem. Res.* **1983**, *16*, 161.
(18) Gutsche, C. D. *Calixarenes*; Kluwer Academic Publishers: Dordrecht, 2001; Chapter 1 and references therein.
(19) See, for example: (a) Petrella, A. J.; Raston, C. L. *J. Organomet. Chem.* **2004**, *689*, 4125. (b) Homden, D. M.; Redshaw, C. *Chem. Rev.* **2008**, *108*, 5086. (c) Aronica, C.; Chastanet, G.; Zueva, E.; Borshch, S. A.; Clemente-Juan, J. M.; Luneau, D. *J. Am. Chem. Soc.* **2008**, *130*, 2365.
(20) (a) Karotsis, G.; Teat, S. J.; Wernsdorfer, W.; Piligkos, S.; Dalgarno, S. J.; Brechin, E. K. *Angew. Chem., Int. Ed.* **2009**, *48*, 8285. (b) Karotsis, G.; Kennedy, S.; Dalgarno, S. J.; Brechin, E. K. *Chem. Commun.* **2010**, *46*, 3884. (c) Karotsis, G.; Evangelisti, M.; Dalgarno, S. J.; Brechin, E. K. *Angew. Chem., Int. Ed.* **2009**, *48*, 9928.
(21) Aronica, C.; Chastanet, G.; Zueva, E.; Borshch, S. A.; Clemente-Juan, J. M.; Luneau, D. *J. Am. Chem. Soc.* **2008**, *130*, 2365.
(22) (a) Desroches, C.; Pilet, G.; Borshch, S. A.; Parola, S.; Luneau, D. *Inorg. Chem.* **2005**, *44*, 9112. (b) Desroches, C.; Pilet, G.; Szilágyi, P. A.; Molnár, G.; Borshch, S. A.; Bousseksou, A.; Parola, S.; Luneau, D. *Eur. J. Inorg. Chem.* **2006**, 357. (c) Kajiwara, T.; Iki, N.; Yamashita, M. *Coord. Chem. Rev.* **2007**, *251*, 1734. (d) Bi, Y.; Wang, X.-T.; Liao, W.; Wang, X.; Wang, X.; Zhang, H.; Gao, S. *J. Am. Chem. Soc.* **2009**, *131*, 11650. (e) Bilyk, A.; Dunlop, J. W.; Fuller, R. O.; Hall, A. K.; Harrowfield, J. M.; Wais Hosseini, M.; Koutsantonis, G. A.; Murray, I. W.; Skelton, B. W.; Stamps, R. L.; White, A. H. *Eur. J. Inorg. Chem.* **2010**, 2106. (f) Bilyk, A.; Dunlop Hall, A. K.; Harrowfield, J. M.; Wais Hosseini, M.; Koutsantonis Skelton, B. W.; White, A. H. *Eur. J. Inorg. Chem.* **2010**, 2089. (g) Bilyk, A.; Dunlop, J. W.; Fuller, R. O.; Hall, A. K.; Harrowfield, J. M.; Wais Hosseini, M.; Koutsantonis, G. A.; Murray, I. W.; Skelton, B. W.; Sobolev, A. N.; Stamps, R. L.; White, A. H. *Eur. J. Inorg. Chem.* **2010**, 2127.

magnets (SMMs, Figure 1B),[20a] enneanuclear Cu^{II} tricapped trigonal prismatic clusters that act as versatile anion binding materials (Figure 1C),[20b] and a [$Mn^{III}_4Gd^{III}_4$] cluster that displays an enhanced MCE.[20c] This paper extends our original communication on the latter and describes the syntheses, structures, and magnetic properties of a family of [$Mn^{III}_4Ln^{III}_4$] clusters, the first methylene-bridged calix[*n*]arene-based 3d/4f molecules, in which the replacement of one Ln(III) ion for another invokes dramatic changes in the observed magnetic properties in otherwise structurally analogous molecules.

Experimental Details

$Mn(NO_3)_2 \cdot 4H_2O$ (0.1 g, 0.39 mmol), $Gd(NO_3)_3 \cdot 6H_2O$ (0.1 g, 0.22 mmol), and C4 (0.1 g, 0.23 mmol) were dissolved in a mixture of dimethylformamide (DMF) (10 cm^3) and MeOH (10 cm^3). Following 5 min of stirring, NEt_3 (0.2 g, 1.97 mmol) was added dropwise, and the resulting purple solution was stirred for a further hour. X-ray quality crystals were obtained in good yield (40%) after slow evaporation of the mother liquor. Elemental analysis (%) calculated for **1**, $C_{130}H_{140}Mn_4Gd_4N_8O_{40}$: C, 47.27; H, 4.27; N, 3.39. Found: C, 47.02; H, 4.14; N, 3.27.

Complexes **2** and **3** were made in an analogous manner using $Tb(NO_3)_3 \cdot 6H_2O$ and $Dy(NO_3)_3 \cdot 6H_2O$, respectively, in place of $Gd(NO_3)_3 \cdot 6H_2O$. Elemental analysis (%) calculated for **2**, $C_{135}H_{155}Mn_4Tb_4N_9O_{43}$: C, 47.04; H, 4.53; N, 3.66. Found: C, 46.98; H, 4.24; N, 3.59. Elemental analysis (%) calculated for **3**, $C_{130}H_{140}Mn_4Dy_4N_8O_{40}$: C, 46.97; H, 4.24; N, 3.37. Found: C, 46.51; H, 4.18; N, 3.25.

General Crystallographic Details. Data for **1**[20c] and **2** were collected on a Bruker Nonius X8 Apex II diffractometer operating with Mo Kα radiation ($\lambda = 0.71073$ Å) at $T = 100(2)$ K. Data for **3** were collected on a Bruker Apex II CCD diffractometer operating with synchrotron radiation ($\lambda = 0.77490$ Å) at $T = 100(2)$ K. The routine SQUEEZE was applied to the data for **1**−**3** due to the presence of badly disordered solvent molecules.[23] In all cases, this had the effect of dramatically improving the agreement indices.

Crystal Data for 1:[20c] $C_{130}H_{122}Gd_4Mn_4N_8O_{42}$, $M = 3317.12$, black block, 0.25 × 0.20 × 0.18 mm^3, monoclinic, space group *C*2/*c* (No. 15), $a = 34.41(3)$, $b = 12.397(9)$, and $c = 32.15(4)$ Å, $\beta = 98.14(3)°$, $V = 13576(22)$ $Å^3$, $Z = 4$, $2\theta_{max} = 46.8°$, 56 018 reflections collected, 9621 unique ($R_{int} = 0.0831$), final GooF = 1.015, $R1 = 0.0462$, $wR2 = 0.1217$, R indices based on 7169 reflections with $I > 2\sigma(I)$ (refinement on F^2).

Crystal Data for 2: $C_{135}H_{155}Mn_4N_9O_{43}Tb_4$, $M = 3447.12$, black block, 0.40 × 0.32 × 0.28 mm^3, triclinic, space group $P\bar{1}$ (No. 2), $a = 17.87(5)$, $b = 19.62(5)$, and $c = 23.80(7)$ Å, $\alpha = 102.46(4)$, $\beta = 104.83(4)$, and $\gamma = 96.28(4)°$, $V = 7754(37)$ $Å^3$, $Z = 2$, $2\theta_{max} = 46.5°$, 143 013 reflections collected, 21 725 unique ($R_{int} = 0.0857$), final GooF = 0.977, $R1 = 0.0507$, $wR2 = 0.1290$, R indices based on 14 442 reflections with $I > 2\sigma(I)$ (refinement on F^2).

Crystal Data for 3: $C_{130}H_{140}Dy_4Mn_4N_8O_{40}$, $M = 3324.26$, purple plate, 0.20 × 0.06 × 0.02 mm^3, triclinic, space group $P\bar{1}$ (No. 2), $a = 17.805(2)$, $b = 19.781(2)$, and $c = 23.563(3)$ Å, $\alpha = 102.752(2)$, $\beta = 104.586(2)$, and $\gamma = 96.203(2)°$, $V = 7714.9(15)$ $Å^3$, $Z = 2$, $D_c = 1.431$ g/cm^3, $F_{000} = 3320$, Bruker Apex II CCD diffractometer, synchrotron radiation, $\lambda = 0.77490$ Å, $T = 100(2)$ K, $2\theta_{max} = 51.1°$, 64 375 reflections collected, 22 184 unique ($R_{int} = 0.0609$), final GooF = 0.921, $R1 = 0.0511$, $wR2 = 0.1219$, R indices based on 15 071 reflections with $I > 2\sigma(I)$ (refinement on F^2), 1764 parameters, 147 restraints. Lp and absorption corrections applied, $\mu = 2.877$ mm^{-1}.

Magnetic Data and Analysis. Magnetization measurements down to 2 K and specific heat measurements using the relaxation method down to 0.3 K on powdered crystalline samples of **1**−**3** were carried out by means of commercial setups for the 0−9 T magnetic field range. Ac-susceptibility measurements were extended down to 80 mK with a homemade susceptometer, installed in a dilution refrigerator.

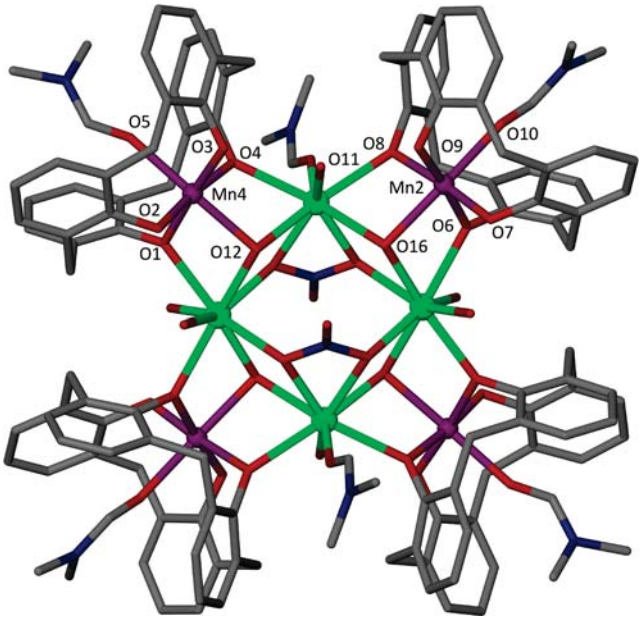

Figure 2. Molecular structure of **1**, showing the coordination environments around the Mn^{III} and Gd^{III} centers. Hydrogen atoms, hydroxide anions, and cocrystallized DMF molecules are omitted for clarity. Color code as in Figure 1; Ln, green.

Results and Discussion

The reaction of $Mn(NO_3)_2 \cdot 4H_2O$ and $Ln(NO_3)_3 \cdot 6H_2O$ with C4 and NEt_3 in a solvent cocktail of MeOH/DMF results in the formation of complexes with the general formula [$Mn^{III}_4Ln^{III}_4$-$(OH)_4(C4)_4(NO_3)_2(DMF)_6(H_2O)_6](OH)_2$, where Ln = Gd (**1**), Tb (**2**), or Dy (**3**). Crystals of **1** are in the monoclinic space group *C*2/*c*, while those of **2** and **3** are found to crystallize in the triclinic space group $P\bar{1}$. The C4-supported clusters in all three complexes are structurally analogous, differing only in the number of cocrystallized solvent molecules (which are badly disordered), and so for the sake of brevity we will limit our discussion to complex **1**, highlighting any specific differences between the molecules at appropriate stages. The cluster (Figure 2) comprises a near-planar octametallic core describing a "square" of Mn(III) ions encasing a "square" of Gd(III) ions. The {Mn_4} square has dimensions 6.591 × 7.042 Å and the {Gd_4} square 3.915 × 3.929 Å, with the latter rotated approximately 45° with respect to the former. This is a very unusual motif but has also been observed recently in the cluster $[Mn_4Nd_4(OH)_4(fcdc)_2(Piv)_8(bdea)_4] \cdot H_2O$ (fcdc = ferrocene dicarboxylate; piv = pivalate or trimethylacetate; $bdeaH_2$ = *N*-butyldiethanolamine).[24] The central [$Gd^{III}_4(OH)_4(NO_3)_2$] unit comprises the four Gd(III) ions connected to each other via four μ_3-OH^- ions (O12 and O16 and symmetry equivalents) and two η^2,η^2,μ_3-NO_3^- ions. The OH^- ions also bridge to the four [Mn^{III}(C4)(DMF)] corner units of the {Mn_4} square. The μ_3-TBC4 ligands are fully deprotonated with two oxygen atoms (O1, O4 and O7, O8 and symmetry equivalents) bonding terminally to the Mn(III) ions and two (O2, O3 and O6, O9 and symmetry equivalents) μ-bridging to the central {Gd_4}

(23) Spek, A. L. *Acta Crystallogr.* **1990**, *A46*, C34.

(24) Mereacre, V.; Ako, A.; M.; Filoti, G.; Bartolomé, J.; Anson, C. E.; Powell, A. K. *Polyhedron* **2010**, *29*, 244.

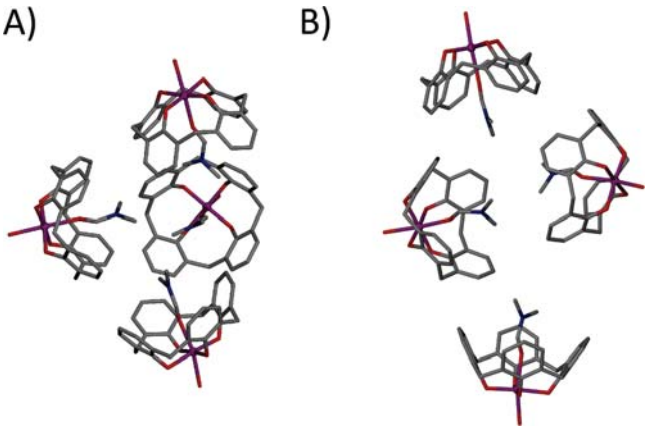

Figure 3. Partial extended structures of **1** (A) and **2** (and isostructural **3**, B), showing the packing of [Mn(III)−C4] subunits in each case. (A) Four corner units of nearest-neighbor clusters form a pseudocapsule assembly containing a DMF microenvironment that is reminiscent of other calixarene-based molecular capsules.[16a,c,e] (B) Three corner units of nearest-neighbor clusters form a related assembly, albeit with one pointing away from the DMF microenvironment relative to that shown in panel A. Figures are not to scale.

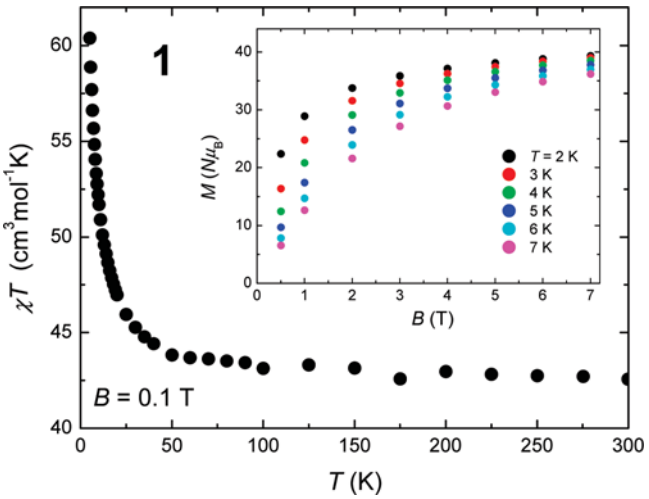

Figure 4. Temperature dependence (5−300 K) of the dc-susceptibility for **1** collected in an applied field of 0.1 T. Inset: magnetization of **1** versus applied field for several temperatures.

square. The Mn ions lie in distorted octahedral geometries in $\{O_6\}$ coordination spheres with the Jahn−Teller axes (O10−Mn2, 2.225 Å; Mn2−O16, 2.218 Å; O5−Mn4, 2.261 Å; Mn4−O12, 2.221 Å) described by the DMF−Mn−OH vectors, i.e., across the diagonal of the $\{Mn_4\}$ square. The Gd(III) ions are eight-coordinate and are in distorted square antiprismatic geometries, with their remaining coordination sites filled by a combination of terminal H_2O molecules, which form intramolecular H-bonds to the terminally bonded O-atoms of the C4 ligands (e.g., O8···O11, 2.642 Å) and intermolecular H-bonds to hydroxide anions, and DMF molecules.

Examination of the extended structures of **1**−**3** shows that symmetry-equivalent clusters pack together to form two types of complex arrangement. Disorder is present in the solvent molecules cocrystallized with the clusters in each of the crystal lattices, and this is severe enough to preclude detailed analysis of the intermolecular interactions between all of the structural components in each crystal structure. The structure of **1** differs from those of **2** and **3** (isostructural), and packing of the asymmetric unit shows that four [Mn(III)−C4] subunits assemble in a pseudocapsule assembly to produce a DMF-rich microenvironment between the corner units of nearest-neighbor clusters (Figure 3A). These are reminiscent of hexameric calixarene-based molecular capsules and suggest that appropriately functionalized C4 molecules could be employed in cluster formation to invoke templated self-assembly into nanometer-scale assemblies containing large internal volumes.[16a,c,e] The extended structures of isostructural **2** and **3** (Figure 3B) show the formation of a similar type of pseudocapsule assembly. Three [Mn(III)−C4] subunits assemble to produce a second type of DMF microenvironment, while the fourth neighboring subunit points away from the center of the capsule-like assembly. Notably, the [Mn(III)−C4] subunit found in the $[Mn^{III}_2Mn^{II}_2]$ SMM shown in Figure 1B is preserved in these new hybrid 3d/4f complexes. This indicates that this is indeed a favorable structural subunit (or "metalloligand") for Mn(III) and that these moieties may well be exploited in the formation of other complexes and supramolecular architectures whose self-assembly may be governed by relatively small changes in reaction conditions.

Magnetic Studies

We investigated the magnetic properties of **1** by dc-susceptibility experiments in the temperature range from 300 to 5 K in an applied field $B = 0.1$ T (Figure 4). The room-temperature χT value of ∼42.8 cm^3 K mol^{-1} is close to the spin-only ($g = 2.0$) value expected for an uncoupled $[Mn^{III}_4Gd^{III}_4]$ unit, ∼43.5 cm^3 K mol^{-1}. The value stays essentially constant as the temperature is decreased until approximately 50 K, below which it increases, reaching a maximum of ∼60.5 cm^3 K mol^{-1} at 5 K. This behavior is suggestive of very weak intramolecular exchange, and one would expect a nesting of, and thus population of, several S states even at the lowest temperatures studied. This is reflected in the low-temperature χT value, which is well below that expected for a ferromagnetically coupled cluster with an isolated $S = 22$ ground state (253 cm^3 K mol^{-1}), and can also be seen in the magnetization versus field data (collected in the 2−7 K temperature range for applied fields up to 7 T, and plotted in the inset of Figure 4), which shows M increasing only slowly with B rather than quickly reaching saturation as one would expect for an isolated spin ground state. This is indicative of the population of low-lying levels with smaller magnetic moment, which only become depopulated with the application of a large field. This result suggests **1** to be an excellent candidate for magnetic refrigeration.[15b] To validate this statement, our preliminary studies focused on the determination of the magnetic entropy change, ΔS_m, of **1** by analyzing the experimental $M(B)$ data of Figure 4. In an isothermal process of magnetization, ΔS_m can be derived from the Maxwell relations by integrating over the magnetic field change $\Delta B = B_f - B_i$, i.e., $\Delta S_m(T)_{\Delta B} = \int[\partial M(T,B)/\partial T]_B \, dB$.[1,2,5] The so-obtained ΔS_m is depicted in Figure 5 for several field changes. It can be seen that $-\Delta S_m$ increases gradually with increasing ΔB, reaching a value of 19.0 J kg^{-1} K^{-1} at $T = 4$ K, achieved for the experimentally accessible maximum ΔB of 7 T. This is among the highest values ever reported for this temperature range.[5] We also note that the observed magnetic entropy changes are much larger than the maximum allowable entropy for an

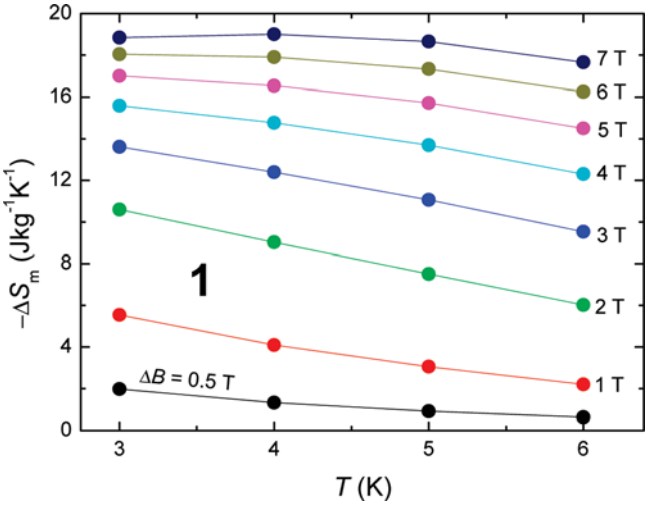

Figure 5. Temperature dependencies of the magnetic entropy change of **1** for applied field changes ΔB.

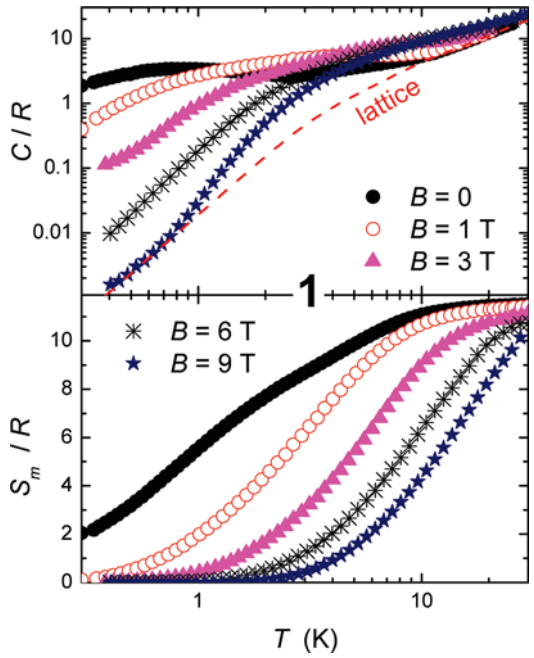

Figure 6. Top: temperature dependencies of the heat capacity of **1** normalized to the gas constant R collected for B = 0, 1, 3, 6, and 9 T. Dashed line is the fitted lattice contribution. Bottom: temperature dependencies of the experimental magnetic entropy for several B, as obtained from the respective magnetic contributions to the total heat capacity.

isolated $S = 22$ spin ground state, i.e., $R \ln(2S + 1) = 3.8R = 9.0$ J kg^{-1} K^{-1}. This demonstrates that the presence of low-lying excited spin states can have a strong and positive influence on the MCE.[5]

We next turn to the study of the MCE of **1** by means of heat capacity (C) experiments, emphasizing that the measurement of the heat capacity as a function of temperature in constant magnetic field provides the most complete characterization of the MCE in magnetic materials.[2,5] The top panel of Figure 6 depicts the experimental heat capacity curves of **1** in the temperature range from 30 to 0.3 K for several applied fields. It can be seen that the curves collected at temperatures below 1 K are strongly dependent on the applied field span over 3 orders of magnitude in units of R for the investigated field changes. The zero-field curve achieves a maximum of ~4R for

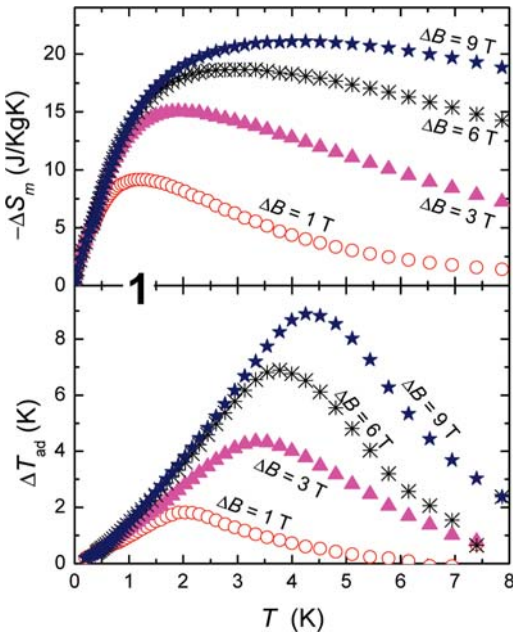

Figure 7. Top: temperature dependencies of the magnetic entropy change of **1** for the indicated applied-field changes ΔB. Bottom: temperature dependencies of the adiabatic temperature change of **1** for the indicated ΔB. Both $\Delta S_m(T,\Delta B)$ and $\Delta T_{ad}(T,\Delta B)$ curves are obtained from the heat capacity data of Figure 6.

$T = 0.8$ K, while the field-independent lattice contribution has a value of $6 \times 10^{-3}R$ for the same temperature. The relevant feature is the broad specific heat anomaly that shifts toward higher temperatures on increasing applied field; we attribute this to the field-splitting of the spin multiplets of the molecule. We stress, however, that this behavior cannot be reproduced by a simple model based on a well-defined $S = 22$ spin ground state (which would not exceed ~1R). To explain the excess of experimental heat capacity, we need to invoke the contribution arising from the population of low-lying excited spin states, corroborating the previous magnetization experiments. In the high-temperature range, a large field-independent contribution appears that can be attributed to the lattice phonon modes of the crystal. The dashed line in the top panel of Figure 6 represents a fit to this contribution with the well-known low-temperature Debye function, yielding a value of $\Theta_D = 23$ K for the Debye temperature, typical for this class of cluster complex.[1b]

From the experimental heat capacity, the temperature dependence of the magnetic entropy S_m is obtained by integration, i.e., using $S_m(T,B) = \int C_m/T \, dT$, where the magnetic heat capacity C_m is obtained from C upon subtracting the lattice contribution. The so-obtained S_m is shown in the bottom panel of Figure 6 for the corresponding applied fields. As further evidence of the participation of excited spin states, we note that the experimental $S_m(T)$ by far exceeds the value expected for an isolated $S = 22$ ground state, i.e., 3.8R.

It now becomes straightforward to obtain the magnetic entropy changes ΔS_m of **1**, whose temperature dependencies are depicted in the top panel of Figure 7 for several field changes. Any uncertainty in the determination of the field-independent lattice contribution is irrelevant for this calculation and cancels out since we are dealing with differences between entropies. The $\Delta S_m(T,\Delta B)$ curves are consistent with the preliminary estimates obtained in Figure 5, proving the validity of employing both the magnetization and heat capacity data in the analysis.

Furthermore, we observe that $-\Delta S_m$ reaches the extremely very large value of 21.3 J kg^{-1} K^{-1} at liquid-helium temperature for the investigated field change, ΔB from 9 to 0 T.

Analysis of the heat capacity data also permits us to estimate the adiabatic temperature change ΔT_{ad} by using $\Delta T_{ad}(T)_{\Delta B} = [T(S_m)_{B_f} - T(S_m)_{B_i}]S_m$ directly from the experimental magnetic entropy S_m depicted in Figure 6 (bottom panel). The bottom panel of Figure 7 shows that the maximum in ΔT_{ad} gradually decreases and shifts to lower temperatures with decreasing field change ΔB. Indeed, it changes from $\Delta T_{ad} = 9.0$ K for ΔB from 9 to 0 T at $T = 4.4$ K to $\Delta T_{ad} = 2.0$ K for ΔB from 1 to 0 T at $T = 2.0$ K. In other words, the magnetic field dependence of the adiabatic temperature change increases from 1 to 2 K/T, respectively, making **1** one of the finest refrigerants in the liquid-helium temperature range.[2,15b]

We have stressed throughout the text that negligible anisotropy is a major requirement for achieving an enhanced MCE with polymetallic molecules. As is well established, a large magnetic anisotropy promotes SMM behavior, for which slow relaxation of the net spin per molecule is obtained below a superparamagnetic blocking temperature. The consequence is that the blocked molecular spins tend to lose thermal contact with the lattice at low temperatures,[25] resulting in a lower magnetic entropy and therefore a lower MCE. The effect of the anisotropy on the efficiency of a polymetallic molecule in terms of magnetic refrigeration has already been demonstrated by means of simple numerical simulations, and experimentally using a large variety of molecules from the prototype Mn_{12} SMM to the [ideally] isotropic Mn_{10} supertetrahedron.[5] However, to the best of our knowledge, no example has yet been provided of a molecular refrigerant in which the degree of anisotropy can be experimentally and exclusively altered/tuned without structural alteration. The [$Mn^{III}_4Ln^{III}_4$] molecular cluster can provide such a playground since the identity of the Ln(III) can be easily changed. By replacing the zero-orbital moment Gd^{III} ion (**1**) with the anisotropic Tb^{III} (**2**) or Dy^{III} (**3**) ion, one can expect to observe abrupt changes in the magneto-thermal properties of these otherwise structurally analogous molecules.

Figure 8 depicts the dc-susceptibility measurements for **2** and **3**, collected in the temperature range from 300 to 2 K for an applied field $B = 0.1$ T. Let us first examine complex **2**; terbium(III) is a non-Kramers ion with a $^7F_6$ ground state. The fit of the experimental $\chi(T)$ data to the Curie−Weiss law in the temperature range from 300 to 5 K provides a small $\theta = -0.16$ K, suggesting that the metallic ions are only weakly magnetically correlated. The room-temperature χT value for **2** is ∼55.5 cm^3 K mol^{-1}, in reasonable agreement with the spin-only ($g = 2.0$) value expected for an uncoupled [$Mn^{III}_4Tb^{III}_4$] unit of ∼59.3 cm^3 K mol^{-1}. The value stays essentially constant as the temperature is decreased until approximately 150 K, below which it decreases smoothly down to 22 K, reaching a value of ∼52.3 cm^3 K mol^{-1}. The temperature range from 22 to 7 K is marked by an upward shift in the χT value that, considering the relatively large intercluster spacing, we associate with ferro- or ferrimagnetic intramolecular exchange. In the lowest temperature range, χT decreases sharply to ∼43.5 cm^3 K mol^{-1} at 2 K, suggesting either antiferromagnetism or, perhaps more likely, the progressive depopulation of excited states of the lanthanide ions. A similar conclusion may be drawn by looking at the field dependence of the magnetization (inset of Figure 8, top panel). With increasing field, the onset of a net molecular moment promotes a relatively quick increase of the magnetization, reaching $20.5N\mu_B$ at $B = 1$ T for $T = 2$ K, after which it increases linearly without saturating. Likewise for **3**, we expect the crystal field to split the $^6H_{15/2}$ ground state of dysprosium(III). Contrary to **2**, the fit of the experimental $\chi(T)$ data to a Curie−Weiss law in the temperature range from 300 to 5 K provides a very small but positive value ($\theta = +0.35$ K), suggesting that the ferro- or ferrimagnetic component is relatively stronger in **3**. The $\chi T(T)$ value stays essentially constant from room temperature down to nearly 100 K, below which it experiences a small decrease to ∼66.8 cm^3 K mol^{-1} at $T = 12.6$ K. The lowest temperature range is then characterized by an abrupt increase in χT, which reaches ∼79.5 cm^3 K mol^{-1} at $T = 2$ K, corroborating the presence of a stronger ferro- or ferrimagnetic interaction than observed in **2**. This is also supported by the larger experimental values of the magnetization, whose field dependence (qualitatively) is very similar to that of **2** (inset of Figure 8, bottom panel).

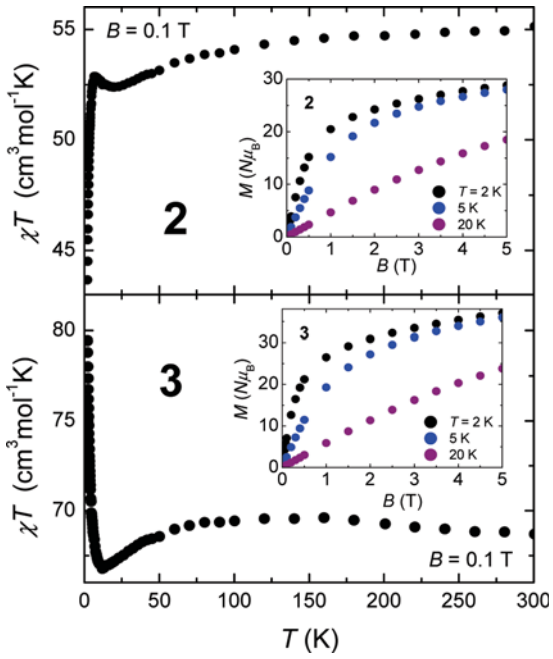

Figure 8. Temperature dependence (5−300 K) of the dc-susceptibility for **2** (top) and **3** (bottom) collected in an applied field of 0.1 T. Insets: magnetization of **2** (top) and **3** (bottom) versus applied field for $T = 2$, 5, and 20 K.

Because of the anisotropy induced by the Tb^{III} and Dy^{III} ions, and the observation that each molecular unit develops a net magnetic moment at low temperatures, it is reasonable to expect superparamagnetic behavior. We therefore investigated the dynamic properties of **2** and **3** by means of ac-susceptibility experiments. Both complexes show out-of-phase signals (χ'') at temperatures above 2 K (Figure S1, Supporting Information), indicative of either a phase transition or slow relaxation of the magnetization. In order to discriminate between these two phenomena, we extended our experiments to the lower temperature region, obtaining the results depicted in Figure 9.

The main feature is a cusp in the in-phase component χ' of the ac-susceptibility which occurs at approximately 0.9 K for both complexes, accompanied by a nonzero out-of-phase component (Figure 9), with both maxima in χ' and χ'' being frequency (f)-dependent. The experimental data suggest superparamagnetic blocking of the molecular spins below T_B,

(25) Evangelisti, M.; Luis, F.; Mettes, F. L.; Aliaga, N.; Aromí, G.; Alonso, J. J.; Christou, G.; de Jongh, L. J. *Phys. Rev. Lett.* **2004**, *93*, 117202.

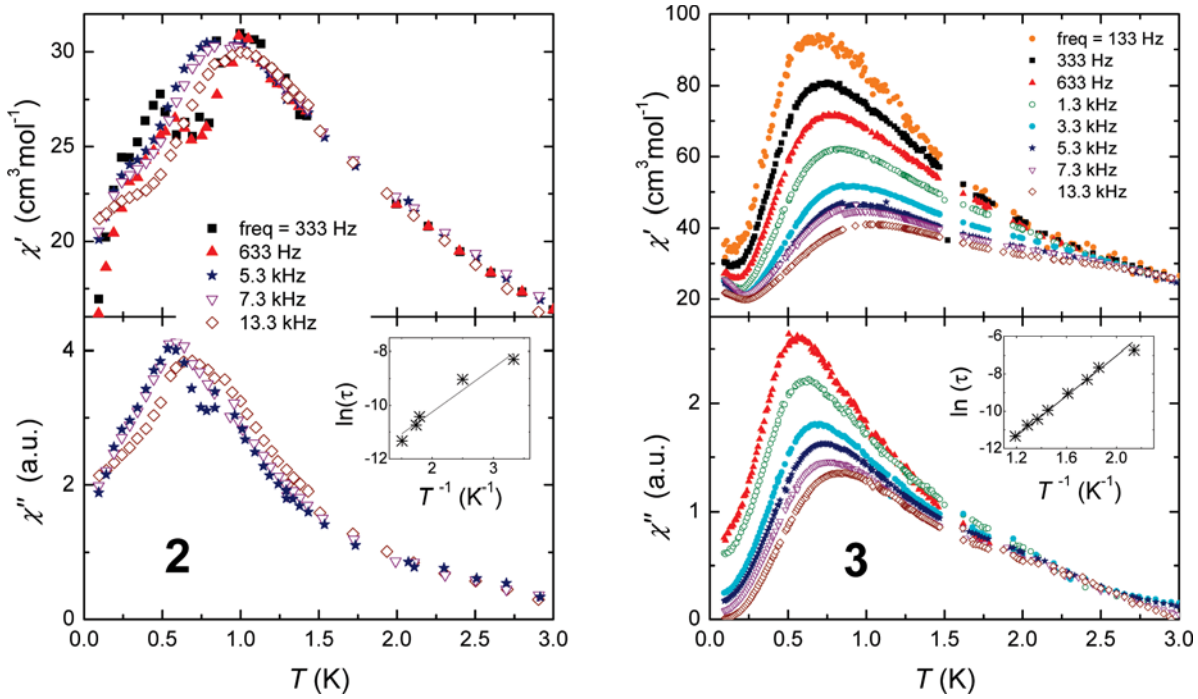

Figure 9. Temperature dependence of the in-phase (χ', top) and out-of-phase (χ'', bottom) ac-susceptibility for **2** (left) and **3** (right), collected in zero-applied field and for the indicated excitation frequencies. Insets: semilogarithmic plots of the (main) zero-field relaxation time. The straight lines are fits to the Arrhenius law.

corresponding to the temperature at maximum absorption. Using the average value $T_B = 0.9$ K, the frequency shift of T_B, nominally $\Delta T_B/(T_B \Delta \log f)$, where ΔT_B is the change in T_B for the given change in frequency $\Delta \log f$, provides values of 0.5 and 0.2 for **2** and **3**, respectively, which are comparable to those of other superparamagnets.[26] The relaxation time for superparamagnets with an anisotropy barrier U is usually described with the Arrhenius law, typical of a thermal activation process: $\tau = \tau_0 \exp(U/k_BT)$, where $\tau = 1/2\pi f$ and τ_0 is an attempt frequency. We have fitted the cusp in the out-of-phase susceptibility with the above equation. The results are presented in Figure 9 (insets), affording $\tau_0 = 1 \times 10^{-7}$ s and $U/k_B = 3.0$ K for **2**, and $\tau_0 = 3 \times 10^{-8}$ s and $U/k_B = 5.0$ K for **3**. Closer inspection of the low-temperature ac-susceptibility (Figure 9) reveals that the magnetic relaxation in these materials is particularly complex, since other (secondary) relaxation pathways can be spotted besides the main one taking place at 0.9 K. Indeed, for both complexes, a rather broad, frequency-dependent "shoulder" is observed in the 2−3 K temperature range. For **2**, a secondary cusp is observed in $\chi''(T)$ at somewhat higher temperature than that of the main feature. For **3**, the maximum absorption of a faster relaxation mechanism takes place below 80 mK, temperatures not experimentally accessible with our setup.

The frequency dependence of the ac-susceptibility below 3 K suggests that both **2** and **3** are SMMs. Therefore, it is not a surprise that heat capacity experiments performed on **2** and **3** (Figure 10) can detect no sign of long-range magnetic order (in the form of a sharp lambda-like anomaly), a result also expected on the basis of structure considerations (see above). The complicated magnetic behavior of these materials is also observed in Figure 10. For example, the zero-field C curve of

(26) Mydosh, J. A. *Spin glasses: an experimental introduction*; Taylor and Francis: London, 1993.

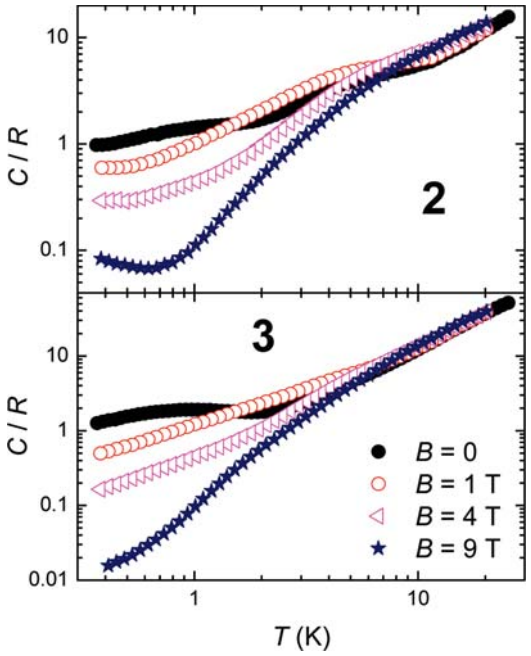

Figure 10. Temperature dependence of the heat capacity normalized to the gas constant R for **2** (top) and **3** (bottom) collected for $B = 0$, 1, 4, and 9 T, as labeled.

complex **2** shows a broad anomaly close to $T = 3$ K, followed by a second one at 1 K, and a third detected at the lowest investigated temperature, the latter being clearly visible in the case of in-field measurements.

The measurements of the heat capacity of **2** and **3** indicate that these molecules would not be suitable for use as molecular refrigerants. This is simply understood by looking at the field-dependent curves and their absolute values in units of R. By comparing the results of Figure 10 with that obtained with an

excellent refrigerant such as **1** (Figure 6), it can be seen that the zero-field heat capacities of **2** and **3** are notably smaller than that of **1** in the (magnetic-dependent) low-temperature region. Furthermore, the change of applied field from 0 to 9 T causes the heat capacities of **2** and **3** to change by 1−2 orders of magnitude at best, i.e., more than an order of magnitude less than in **1**. Likewise, the changes in the magnetic entropy follow the same trend, allowing us to conclude that the anisotropy of the lanthanide ion is of crucial importance for dictating the performance of this family of molecules as magnetic refrigerants.

Conclusions

To conclude, we have expanded our initial studies into $[Mn^{III}_4Ln^{III}_4]$ cluster formation with calixarenes as supporting ligands so that we tailor these 3d/4f clusters of general formula $[Mn^{III}_4Ln^{III}_4(OH)_4(C4)_4(NO_3)_2(DMF)_6(H_2O)_6](OH)_2$ to include either Gd, Tb, or Dy as desired. Magnetic studies show that the $[Mn^{III}_4Gd^{III}_4]$ cluster is an excellent magnetic refrigerant for low-temperature applications. The molecular anisotropy added by replacing Gd with Tb or Dy results in (a) superparamagnetic behavior of the $[Mn^{III}_4Tb^{III}_4]$ and $[Mn^{III}_4Dy^{III}_4]$ clusters with blocking temperatures in the temperature region below 1 K and (b) poor performance of these clusters in terms of magnetic refrigeration. The [Mn(III)−C4] subunit is common to $[Mn^{III}_2$-$Mn^{II}_2]$ SMMs and the $[Mn^{III}_4Ln^{III}_4]$ clusters reported here, and we are currently exploring the use of this moiety in the formation of alternative cluster assemblies through variation in reaction conditions. The substitution of other lanthanides in the $[Mn^{III}_4Ln^{III}_4]$ cluster motif is underway, with a view to fully characterizing the magnetic properties of the entire series of analogous clusters.

Acknowledgment. E.K.B. and S.J.D. thank the EPSRC and Leverhulme Trust for funding and Heriot-Watt University for a studentship (S.K.). M.E. thanks the Spanish Ministry for Science and Innovation for grants MAT2009-13977-C03 and CSD2007-00010. The Advanced Light Source is supported by the Director, Office of Science, Office of Basic Energy Sciences, of the U.S. Department of Energy under contract no. DE-AC02-05CH11231.

Supporting Information Available: Temperature dependence of the out-of-phase ac-susceptibility and crystallographic data (CIF) for **2** and **3**. This material is available free of charge via the Internet at http://pubs.acs.org.

JA104848M